

Supporting Information

On Direct Synthesis of High Quality APbX₃ (A= Cs⁺, MA⁺ and FA⁺; X= Cl⁻, Br⁻ and I⁻) Nanocrystals Following a Generic Approach

Somnath Das and Anunay Samanta*

School of Chemistry, University of Hyderabad, Hyderabad 500046, India

*Corresponding author's Email: anunay@uohyd.ac.in

Contents

Experimental section

Characterization of samples

Scheme: Scheme S1: Reaction steps in the preparation of APbX₃ NCs.

Figures: Fig. S1: Chemical structure of DXDMH.

Fig. S2: PLQY, PXRD pattern and TEM images of the NCs prepared using lower halide content.

Fig. S3: Dependence of PL of the APbBr₃ NCs on reaction temperature.

Fig. S4: Dependence of PLQY and TEM images of the NCs on reaction temperature.

Fig. S5: Batch-to-batch variation of PLQY of the prepared CsPbBr₃ NCs.

Fig. S6: Bright field TEM images, PXRD patterns and UV-Vis absorption spectra of the APbCl₃ NCs.

Fig. S7: Additional TEM images and size distribution histogram of the APbBr₃ NCs.

Fig. S8: Additional TEM images of the APbCl₃ NCs.

Fig. S9: High resolution TEM images of the CsPbCl₃ and CsPbBr₃ NCs.

Fig. S10: High resolution TEM images of FAPbBr₃ NCs.

Fig. S11: Dependence of PLQY of the CsPbCl₃ NCs on Pb:Cl molar precursor ratios.

Fig. S12: UV-Vis absorption and PXRD pattern of the MAPbCl₃ NCs prepared with Pb:Cl molar precursor ratio of 1:3 and 1:1.5.

Fig. S13: PL decay profiles of the MAPbX₃ and FAPbX₃ (X= Cl and Br) NCs.

Fig. S14: PL decay characteristics of the CsPbX₃ NCs prepared with Pb:X molar ratio of 1:2.

Fig. S15: TA spectra and bleach recovery kinetics of the MAPbCl₃ and FAPbCl₃ NCs.

Fig. S16: PL decay profiles of the mixed-halide NCs.

Fig. S17: PL spectra of all mixed-halide NCs directly prepared by our method.

Fig. S18: Bright field TEM images of all mixed-halide NCs.

Fig. S19: PXRD patterns of the mixed-halide NCs.

Fig. S20: PL spectra and digital images of the samples obtained upon post-synthetic reversible halide exchange reactions.

Fig. S21: Post-synthetic cation exchange at A-site on CsPbBr₃ NCs.

Fig. S22: Air- and photo-stability data of the CsPbBr₃ NCs.

Fig. S23: Air- and photo-stability data of the MAPbBr₃ NCs.

Fig. S24: Air- and photo-stability data of the FAPbBr₃ NCs.

Fig. S25: TEM images of the MAPbBr₃ and FAPbBr₃ NCs stored under ambient condition for 80 days.

Fig. S26: Air- and photo-stability data of the CsPbCl₃ NCs.

Fig. S27: Air-stability of the CsPbCl_{1.5}Br_{1.5} and CsPbBr_{1.5}I_{1.5} NCs.

Fig. S28: Stability of MAPbCl₃ and FAPbCl₃ NCs under ambient condition.

Fig. S29: EDX spectra and atomic % ratio of the CsPbBr₃(II) NCs.

Fig. S30: Stability of the CsPbBr₃(II) NCs under ambient condition.

Fig. S31: XPS survey spectra of the CsPbBr₃ NCs.

Fig. S32: Core-level Br 3d XPS spectra of the CsPbBr₃ and CsPbBr₃(II) NCs.

Fig. S33: EDX spectra and corresponding atomic % ratios of CsPbCl₃ and CsPbCl₃(II) NCs.

Fig. S34: PXRD pattern of CsPbCl₃ NCs prepared with Pb:Cl ratio of 1:9.

Fig. S35: ¹H NMR spectra of purified CsPbBr₃(II) NCs in CDCl₃.

Fig. S36: FTIR spectra of the CsPbBr₃ NCs washed with MeOAc.

Tables: Table S1: Optical properties of the APbX₃ NCs on reaction temperature and precursor Pb:X ratio.

Table S2: Comparison of PLQY of the CsPbCl₃ NCs obtained directly by different methods.

Table S3: PL decay parameters of the APbX₃ NCs.

Table S4: Kinetic parameters of the CsPbX₃ NCs obtained from fs-TA studies.

Table S5: Amount of different halide precursors used for direct synthesis of mixed-halide NCs.

Table S6: Optical properties of the mixed-halide NCs.

Table S7: Comparison of the optical properties of mixed-halide NCs with the literature data.

Table S8: PL decay parameters of the mixed-halide NCs.

Table S9: Comparison of the optical properties and stability of APbX₃ NCs with literature data.

Table S10: Advantages and disadvantages of DXDMH and some other popular halide precursors.

Table S11: Atomic % ratios calculated from XPS measurements.

Table S12: Atomic % ratio of CsPbCl₃ NCs with different Pb:Cl ratios obtained from EDX.

Experimental section

Chemicals: Caesium carbonate (Cs₂CO₃, 99.9%), lead oxide (PbO, 99.999%, trace metals basis), formamidinium acetate (99%), 1,3-dichloro-5,5-dimethylhydantoin (DCDMH, 68%), 1,3-diiodo-5,5-dimethylhydantoin (DIDMH, >96%), octadecene (ODE, 90%), oleic acid (OA, technical grade, 90%), oleylamine (OAm, technical grade, 70%), toluene (anhydrous, 99.8%), methyl acetate (MeOAc, anhydrous, 99.5%) and chloroform-d (CDCl₃, 99.8 atom% D) were purchased from Sigma-Aldrich. Methylamine (2M solution in tetrahydrofuran) and 1,3-dibromo-5,5-dimethylhydantoin (DBDMH, 98%) was purchased from TCI chemicals and Lancaster, respectively. Hexane (HPLC & Spectroscopy) and acetonitrile (ACN, dried) were brought from Finar and Merck Chemicals, respectively. All chemicals including the solvents were used without any further purification.

Synthesis of the APbX₃ NCs: Our three-precursor hot injection method of synthesis involves two steps. The first step was preparation of the oleate salt of the ‘A’ cation, which was injected to a solution containing lead and halide precursors at a particular temperature for the preparation of APbX₃ NCs.

Preparation of the oleates: Caesium-oleate (Cs-oleate): Cs-oleate was prepared at high temperature by following a reported procedure of Kovalenko and co-workers with some modifications.¹ In short, 0.16 g of Cs₂CO₃, 6 mL of ODE and 0.55 mL of OA were loaded in a 50 mL two-neck round-bottom (RB) flask, degassed for 5 min at room-temperature and heated under vacuum at 120°C for 1 h. Then the reaction mixture was kept under N₂ atmosphere at this

temperature until all Cs_2CO_3 reacted with OA forming a transparent solution of Cs-oleate. To avoid precipitation at room-temperature, it was preheated at 120°C before use.

Formamidine-oleate (FA-oleate): FA-oleate was also prepared by a reported method with some modifications.² In brief, 0.26 g of FA-acetate was loaded into a 50 mL double-neck RB containing 10 mL of OA (for FAPbCl_3 NCs, a mixture of 4 mL OA and 6 mL ODE is taken) and then degassed for 5 min at room-temperature under vacuum. It was then heated under N_2 atmosphere at 120°C until the entire solution becomes clear. The resultant solution was finally dried under vacuum for 5 min by lowering the reaction temperature to $45\text{-}50^\circ\text{C}$.

Methylammonium-oleate (MA-oleate): Preparation of MA-oleate was quite straightforward and it did not require high temperature. It was obtained by thoroughly mixing 250 μL methylamine (2M in tetrahydrofuran) and 2.5 mL of OA at room-temperature.

Preparation and purification of the CsPbX_3 NCs: In a 50 mL double-neck RB, 0.564 mmol of DBDMH (for CsPbBr_3 NCs) or DCDMH (for CsPbCl_3 NCs) and 0.188 mmol of PbO was loaded along with and 2 mL each of OA and OAm as capping ligands and 5 mL ODE as solvent. The entire mixture was degassed under vacuum at RT for 5 min to remove possible moisture in the mixtures and then heated at 130°C under N_2 environment until a clear solution formed. The reaction temperature was then increased to 210°C and 0.5 mL preheated (at 120°C) Cs-oleate solution was swiftly injected into the reaction medium containing lead and halide precursors. After few seconds (~ 20 sec for CsPbBr_3 NCs and 30 sec for CsPbCl_3 NCs) the reaction system was rapidly cooled in an ice-water bath.

The mixed-halide $\text{CsPb}(\text{Cl}/\text{Br})_3$ and $\text{CsPb}(\text{Br}/\text{I})_3$ NCs were also prepared following a similar procedure employing two different halide precursors. The exact amount of halide precursors used for the synthesis of different systems is listed in Table S5 for convenience.

Purification: The crude reaction product was cooled down to RT, 4 mL hexane was added to it and then centrifuged at 7k rpm for 8 min. The supernatant containing possible unreacted precursors (if any) and solvent was drained out and the precipitate was then dispersed in hexane. After 15 min, the colloidal dispersion was again centrifuged at 7k rpm for 5 min to remove larger particles and possible aggregates and the supernatant solution was collected for further studies. The purification procedure is quite different only for the mixed-halide CsPbBr₂ NCs. In this case, the crude reaction mixture was centrifuged at 3k rpm for 10 min and the precipitate containing larger particles and possible aggregates was removed. Then anhydrous MeOAc as anti-solvent was added drop-wise into the supernatant until turbidity appeared and then quickly centrifuged at 7k rpm for 3 min. The supernatant was discarded, and the precipitate was finally dispersed in hexane for further studies.

MAPbX₃ NCs: In brief, 0.188 mmol of PbO and 0.564/0.282 mmol of DBDMH/DCEMH for the synthesis of MAPbBr₃/MAPbCl₃ NCs were loaded into a double-neck 50 mL RB along with 1.5 mL of OA and 0.5 mL of OAm (for MAPbBr₃) or 2 mL of OA and 0.4 mL of OAm (for MAPbCl₃) in 5 mL of ODE. The reaction mixture was degassed at RT under vacuum for 5 min and after complete solubilization of the reaction mixture at 130°C, the temperature was set to 165°C (for MAPbBr₃) or 95°C (for MAPbCl₃) under N₂ atmosphere. When the reaction temperature reached the desired temperature, MA-oleate (250 μL of methylamine in 2.5 mL of OA) was swiftly injected into reaction medium, followed by rapid quenching (after 20 sec for MAPbCl₃) of the reaction mixture in an ice-water bath to stop the growth of the NCs.

Purification: For MAPbBr₃ NCs, the crude product was brought to RT, 3 mL of MeOAc was added to it and centrifuged at 7k rpm for 6 min. The supernatant containing unreacted precursors and ODE was discarded and the precipitate was dispersed in hexane. After 15 min, it was again

centrifuged at 7k rpm for 5 min and the supernatant was collected for further studies. For MAPbCl₃ NCs, when the crude product reached RT, it was centrifuged at 12k rpm for 7 min after addition of equal volume of MeOAc into it. The supernatant was discarded, and the precipitate was dispersed in hexane for further experiments.

FAPbX₃ NCs: The synthetic strategy and purification procedure for FAPbX₃ NCs was quite similar to that employed for the MAPbX₃ NCs described above. The ligand ratio and reaction temperature used for the preparation of these NCs are listed in Table 1. The only difference in this case was that instead of MA-oleate, 2.5 mL of FA-oleate solution preheated at 100°C was swiftly injected into the reaction medium at the desired temperature for formation of the FAPbX₃ NCs.

RT halide exchange reaction: The halide exchange reactions were performed under ambient condition on colloidal dispersion of pre-synthesized CsPbBr₃ NCs. For this purpose, a saturated solution of DCDMH/DIDMH was prepared in hexane containing OAm and OA. Very small amount (few μL) of the solutions was mixed with a dilute colloidal CsPbBr₃ NCs and shaken vigorously for the anion exchange reactions. An instant reversible change in emission color under UV light (green-to-blue for DCDMH and green-to-red for DIDMH) indicated successful halide exchange reactions.

RT A-site cation exchange: For the post-synthetic cation exchange reaction at RT, we have first diluted 100 μL of FA-oleate solution in 1 mL hexane and added to CsPbBr₃ NCs dispersion of few mM concentrations under stirring and monitored the absorption and PL spectra with different time interval by pipetting out small aliquots from the reaction mixture.

Characterization of samples

Transmission Electron Microscopy (TEM) Measurement: TEM measurements were carried out using Tecnai G2 FE1 F12 transmission electron microscope, which was operated at an accelerating voltage of 200 kV. The samples for this study were prepared by drop-casting a diluted colloidal solution of the NCs on a carbon coated copper-grid and dried overnight under vacuum.

Powder X-ray diffraction (PXRD) Measurement: PXRD patterns of the samples (as thin-films) were recorded on a X-ray diffractometer (Bruker AXS D8) using Cu-K α X-ray radiation ($\lambda = 1.5406 \text{ \AA}$). The samples were prepared by drop-casting highly concentrated colloidal solutions of the NCs on a clean thin quartz glass plate, which was vacuum-dried for 48 h before measurements.

Energy dispersive X-ray (EDX) Measurement: EDX spectra were recorded using Oxford Instruments X-Max^N SDD (50 mm²) system and INCA analysis software. The samples for this measurement were prepared by drop-casting a colloidal solution of the NCs on thin clean quartz plate and they were dried under vacuum for 24h.

X-ray Photoelectron Spectroscopy (XPS) Measurements: XPS measurements were performed in a Thermo Scientific K-Alpha spectrometer equipped with micro-focused monochromatic X-ray source (Al K α , spot size $\sim 400 \text{ \mu m}$) operating at 70 W. The energy resolution of the spectrometer was set at 0.5 eV at pass energy of 50 eV and 5×10^{-5} torr base pressure was maintained at the analysis chamber. Low energy electrons from the flood gun were used for charge compensation. An optimum concentration of the NCs was drop-casted onto a clean quartz glass plate for the XPS measurements and kept under vacuum overnight.

Fourier-Transformed Infrared (FTIR) Measurement: FTIR study was performed using Bruker Tensor II spectrometer. A drop of concentrated colloidal solution of purified CsPbBr₃ NCs was used for this study.

Nuclear Magnetic Resonance (NMR) Measurement: ¹H NMR spectra were recorded by using a NMR (Bruker Avance) spectrometer operating at a frequency of 400 MHz at 25°C. For the preparation of NMR samples, the as-synthesized crude CsPbBr₃ NCs solution in ODE was first centrifuged at 7k rpm for 8 min and the precipitate was dispersed in dried hexane. Then dried MeOAc was added to the NCs dispersion in 1:1 volume ratio, centrifuged at 7k rpm for 5 min and the supernatant was discarded. The precipitate was then dispersed in CDCl₃. A clear solution was used for measuring the ¹H NMR data.

Steady-state Optical Measurements: UV-Vis absorption and photoluminescence (PL) measurements were carried out using spectrophotometer (Cary100, Varian) and spectrofluorimeter (FlouroLog-3, Horiba Jobin Yvon), respectively. For these measurements, a dilute colloidal solution of the NCs (optical density of < 0.05 at the excitation wavelengths in 1 cm path length cuvette) was used.

Time-resolved PL Measurement: These measurements were carried out using a time-correlated single-photon counting (TCSPC) spectrometer (Horiba JobinYvon IBH). The excitation sources were diode lasers emitting at 376/405/481 nm and the detector was an MCP photomultiplier (Hamamatsu R3809U-50). The instrument response function (IRF) of the setup was ~ 61 ps. The decay curves were analyzed by nonlinear least-squares iteration procedure using IBH DAS6 (version 2.2) decay analysis software. The quality of the fits was assessed by the χ^2 values and distribution of the residuals. Further details on the setup can be found elsewhere.³

Ultrafast Transient Absorption (TA) Measurement: These studies were carried out using a setup comprising femtosecond laser sources from Spectra-Physics, USA and spectrometer from CDP systems, Russia. The seed laser output (800 nm, <100 fs, 80 MHz) was directed into a Ti:sapphire regenerative amplifier, which was pumped by the second-harmonic (532 nm) of Nd:YLF laser. A major portion (80%) of the output of the amplifier (800 nm, <120 fs, 1 kHz) was passed through an optical parametric amplifier to generate pump wavelengths for the excitation of APbX₃ NCs. The remaining portion of the output was passed through a variable optical delay line of 4 ns and then directed to a rotating CaF₂ crystal to generate the white probe light. The probe beam was divided into two parts to use as signal and reference beams. The pump and signal beams were focused onto a rotating sample cell maintaining a collinear geometry to obtain a better spatial overlap of the two beams. The transmitted signal and reference beams were received by multichannel photodiode array through a polychromator and further processed to record difference in absorbances (ΔA) as a function of wavelength and pump-probe delay. All TA measurements were performed under low pump density ($J_p = 4-5 \mu\text{J}/\text{cm}^2$) to avoid non-linear optical processes. All TA spectra were chirp-corrected and instrumental resolution was found to be 80-100 fs.⁴

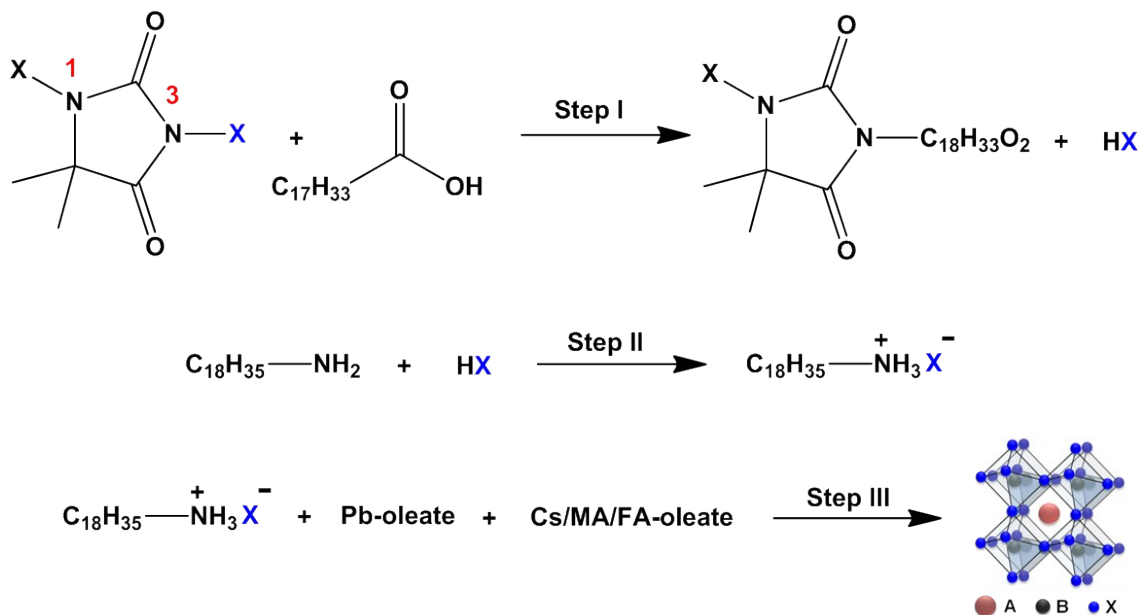
Photoluminescence Quantum Yield (PLQY) Estimation: PLQY of all the samples was calculated using the following equation:

$$QY_S = QY_R \times (I_S/I_R) \times (OD_R/OD_S) \times (\eta_S/\eta_R)^2$$

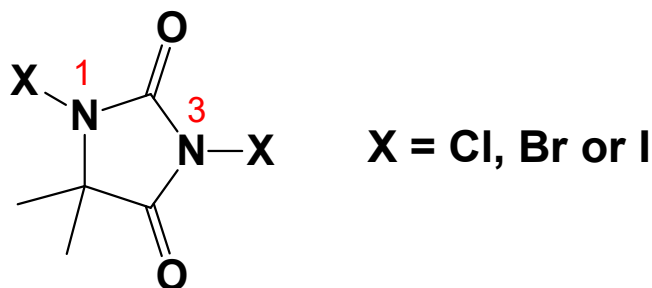
where, I represents the integrated area under the PL spectrum, OD and η represent optical density at the excitation wavelength and refractive index of the medium, respectively. S and R correspond to sample (i.e. the NCs) and reference, respectively. 9,10-diphenylanthracene (PLQY = 0.93 in ethanol),⁵ coumarin-153 (PLQY = 0.54 in ethanol)⁶ and rhodamine 6G (PLQY = 0.95

in water)⁷ were used as reference estimation of PLQY of blue-violet-emitting APbCl₃ and CsPb(Cl/Br)₃ NCs, green-emitting APbBr₃ NCs, yellow-orange-emitting CsPb(Br/I)₃ NCs, respectively.

Photostability and Water Treatment Studies: Photostability of dilute colloidal dispersion of the APbX₃ NCs was studied under continuous illumination of 365 nm UV light (8W) at room-temperature and relative-humidity of 50-60%. For this experiment, a small volume of OA and OAm (30 μL each) was mixed with the purified NCs dispersion in hexane and a small portion of it was diluted in 2.5 mL hexane in a cuvette and placed under the UV light. Then PL intensity of the sample was monitored time-to-time to determine the remnant PL of the NCs. In case of water treatment, additionally, 1 mL of distilled water was put on 2.5 mL of dilute colloidal dispersion of the CsPbBr₃ NCs (in cuvette) and vigorously shaken before starting the experiment.



Scheme S1 Schematic representation of the steps involved in DXDMH-mediated hot injection synthesis of the APbX₃ NCs.



1,3-dihalo-5,5-dimethylhydantoin (DXDMH)

Fig. S1 Chemical structure of 1,3-dihalo-5,5-dimethylhydantoin (DXDMH). ‘X’ represents the halogen atom.

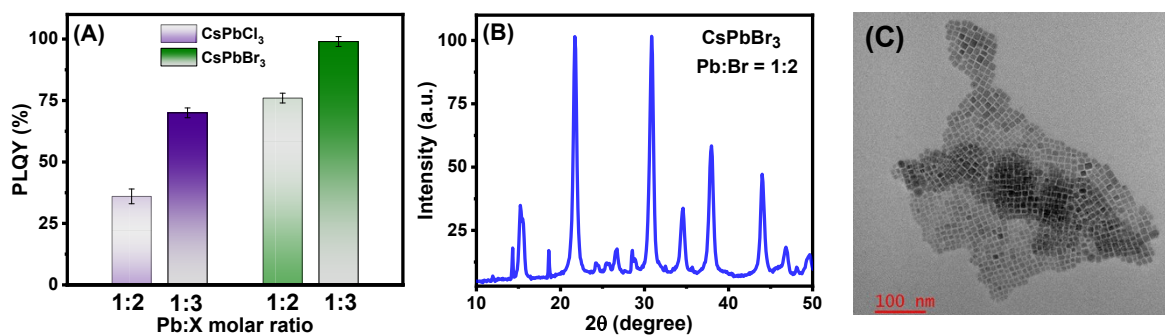


Fig. S2 (A) Dependence of PLQY of the CsPbCl₃ and CsPbBr₃ NCs (obtained at 210°C) on the Pb:X precursor molar ratio. (B) PXRD pattern and (C) TEM image of the samples of CsPbBr₃(II) NCs (prepared using a Pb:Br molar ratio of 1:2). The scale bar is 100 nm.

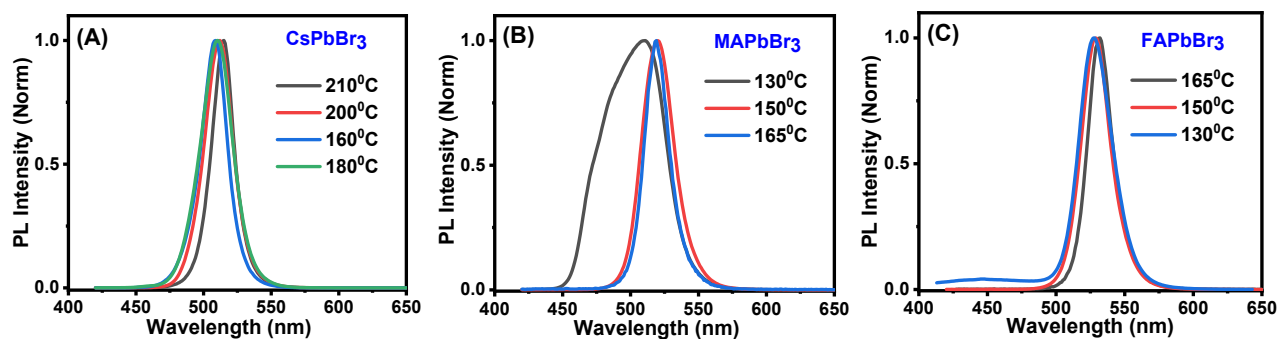


Fig. S3 PL spectra (normalized) of the (A) CsPbBr₃, (B) MAPbBr₃ and (C) FAPbBr₃ NCs obtained at different reaction temperature.

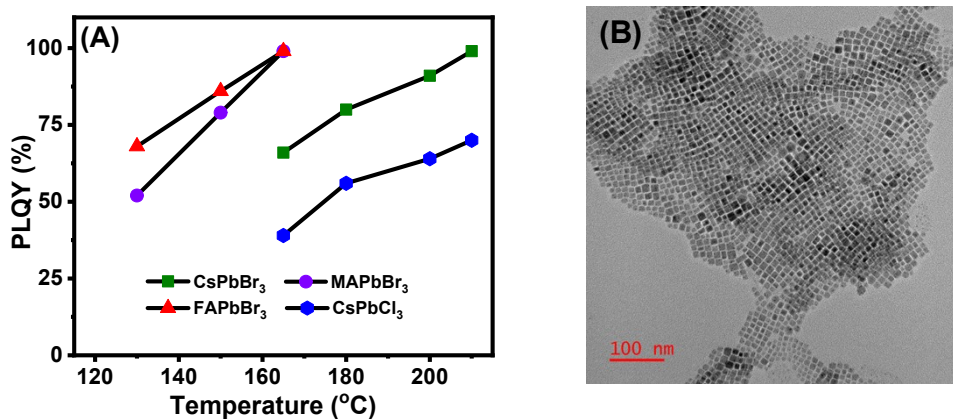


Fig. S4 (A) PLQY of the NCs as a function of reaction temperature. (B) TEM image of the CsPbBr₃ NCs prepared at 180°C. The scale bar is 100 nm.

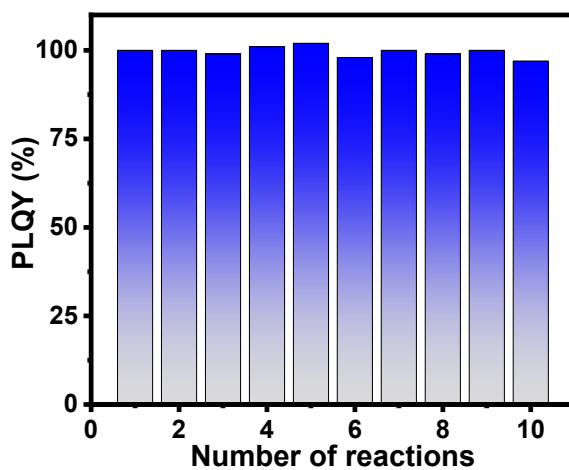


Fig. S5 PLQY of the CsPbBr₃ NCs of different batches highlighting reproducibility of our method.

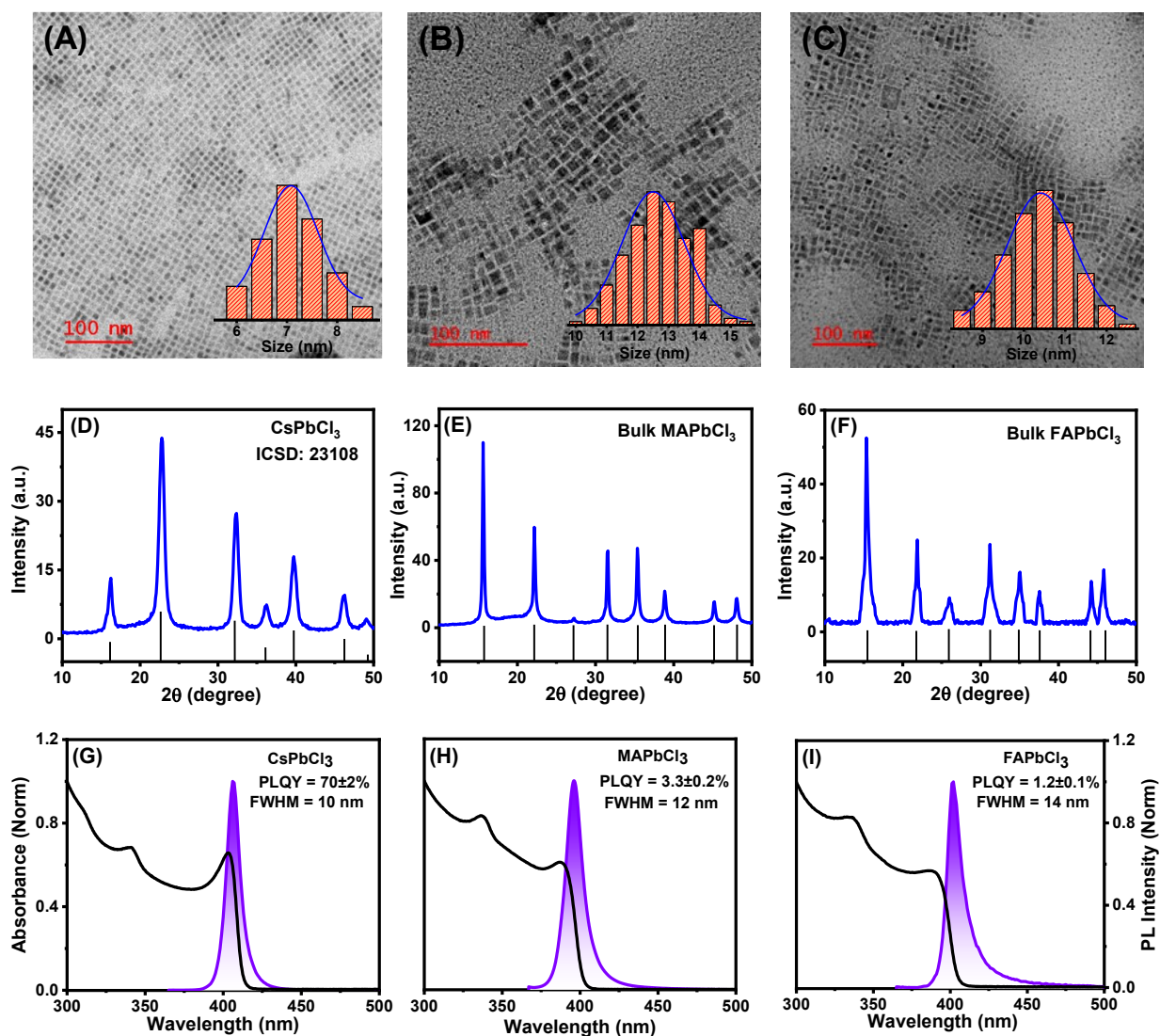


Fig. S6 Bright-field TEM images of (A) CsPbCl₃, (B) MAPbCl₃ and (C) FAPbCl₃ NCs. Inset shows size distribution histogram of the respective NCs. The scale bar is 100 nm for all samples. PXRD patterns of (D) CsPbCl₃, (E) MAPbCl₃ and (F) FAPbCl₃ NCs with reference patterns obtained from their cubic bulk counterparts. UV-Vis absorption and PL spectra of (G) CsPbCl₃, (H) MAPbCl₃ and (I) FAPbCl₃ NCs. The samples were excited at 400 nm.

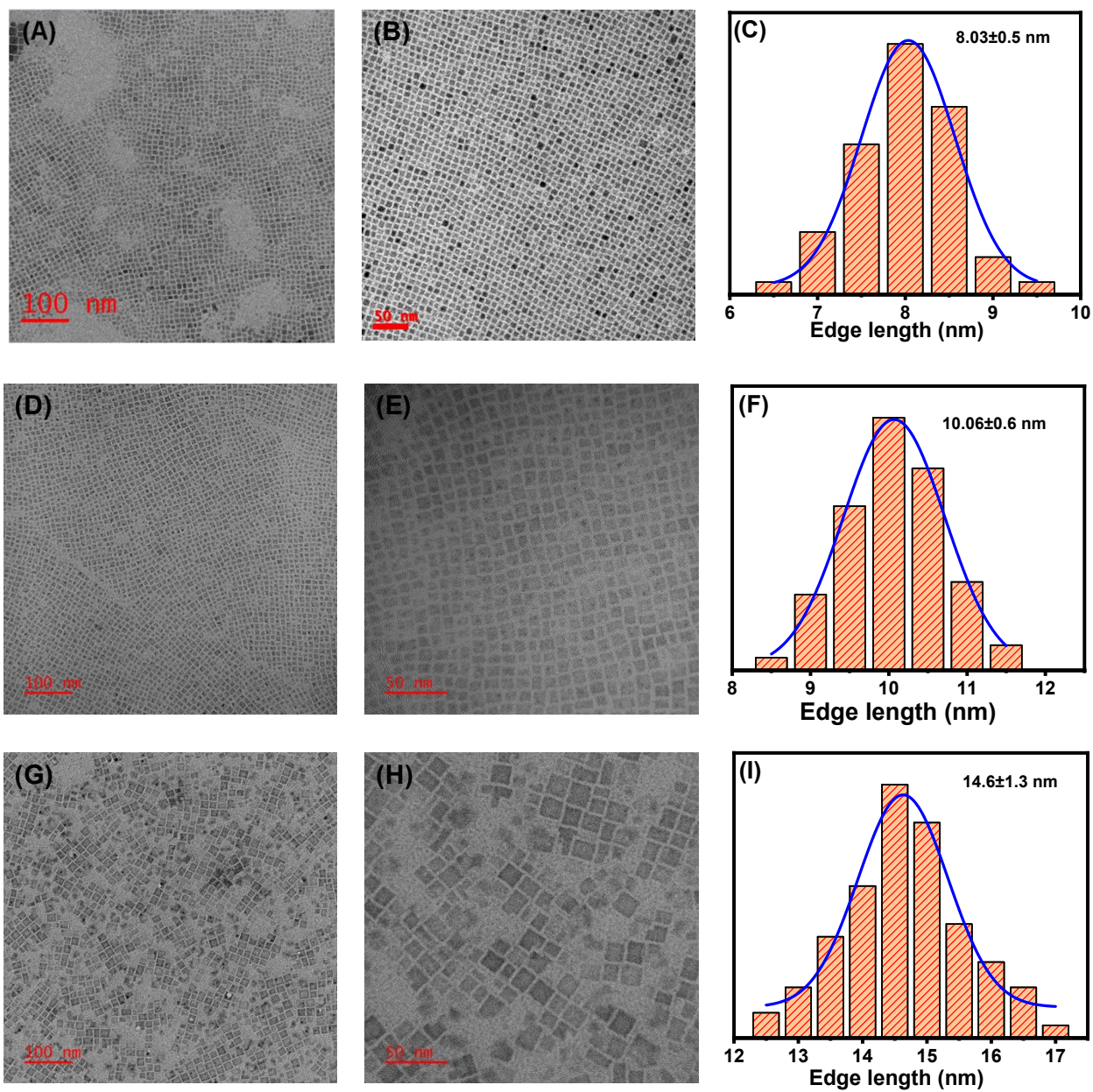


Fig. S7 Additional bright-field TEM images and size distribution histogram of (A-C) CsPbBr₃, (D-F) MAPbBr₃ and (G-I) FAPbBr₃ NCs. The scale bar is indicated at the bottom left corner of each image.

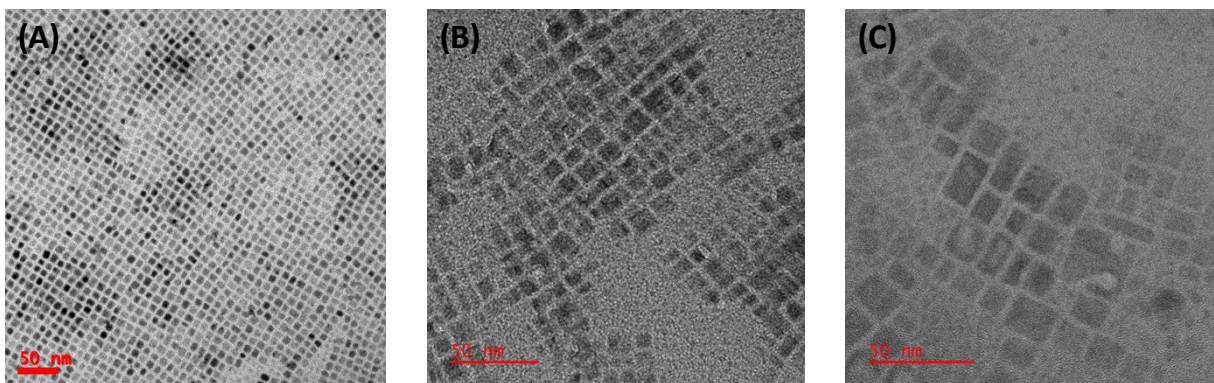


Fig. S8 Additional bright-field TEM images of (A) CsPbCl₃, (B) MAPbCl₃ and (C) FAPbCl₃ NCs. The scale bar is 50 nm in all cases.

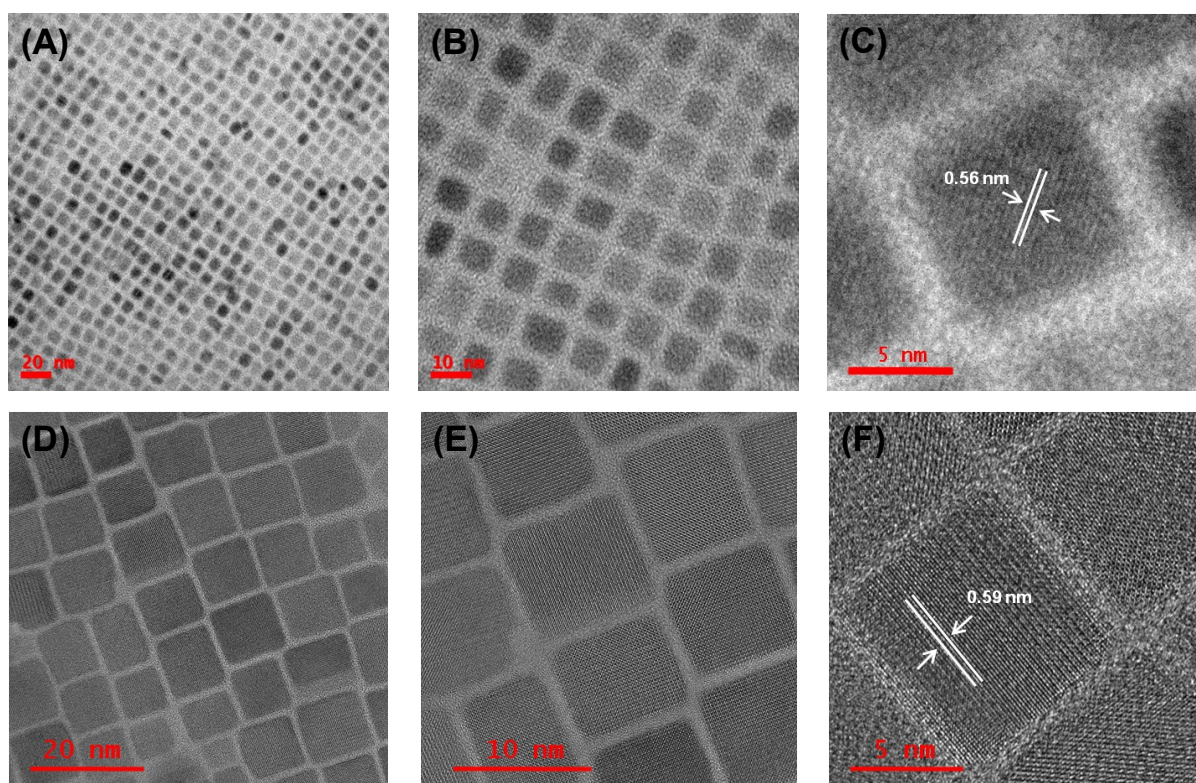


Fig. S9 High-resolution TEM images of (A-C) CsPbCl₃ and (D-F) CsPbBr₃ NCs. The interplanar spacing (d_{100}) corresponding to the (100) planes of the NCs is also measured and shown in Figure C and F. The scale bar is shown in the bottom-left corner of each image.

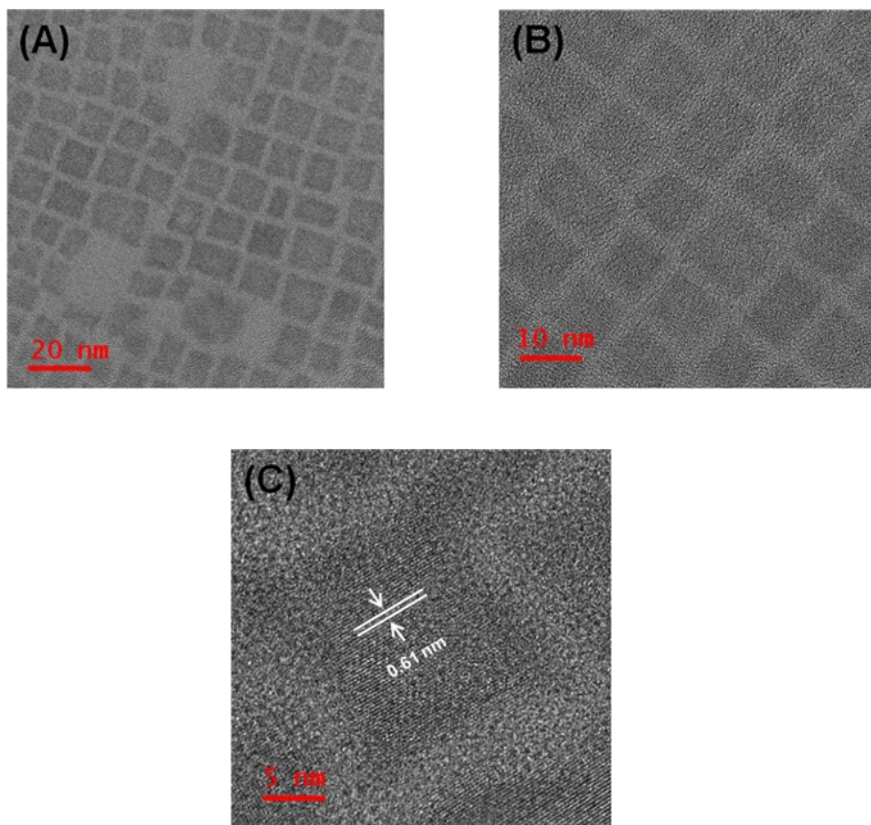


Fig. S10 (A-C) High-resolution TEM images of FAPbBr₃ NCs. The inter-planar spacing (d_{100}) corresponding to the (100) planes of the NCs is also measured and shown in Figure C. The scale bar is shown in the bottom-left corner of each image.

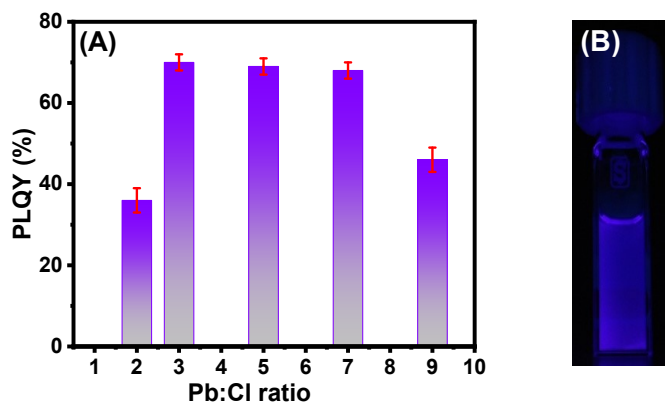


Fig. S11 (A) Dependence of PLQY of the CsPbCl₃ NCs on the Pb:Cl molar precursor ratio. An excess amount of DCDMH is seen to have a detrimental effect on the optical properties of the NCs. (B) Digital image showing the PL of the CsPbCl₃ NCs obtained using Pb:Cl precursor molar ratio of 1:3.

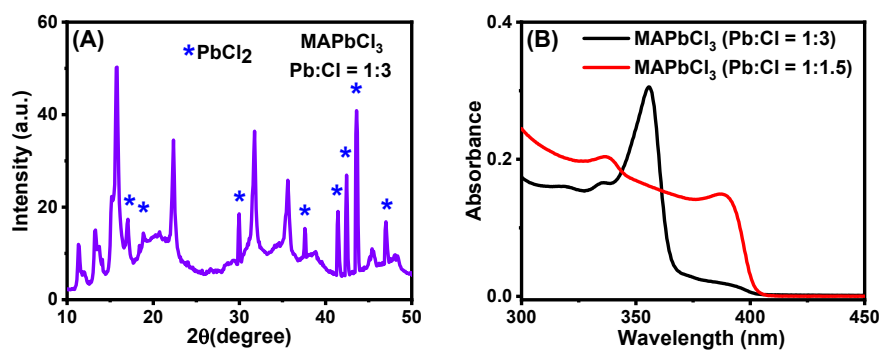


Fig. S12 (A) PXRD pattern of the MAPbCl₃ NCs prepared using 1:3 ratio of Pb:Cl showing the additional diffraction peaks arising from undesired PbCl₂ by-product. (B) Absorption spectra of the MAPbCl₃ NCs prepared using Pb:Cl precursor ratio of 1:3 and 1:1.5.

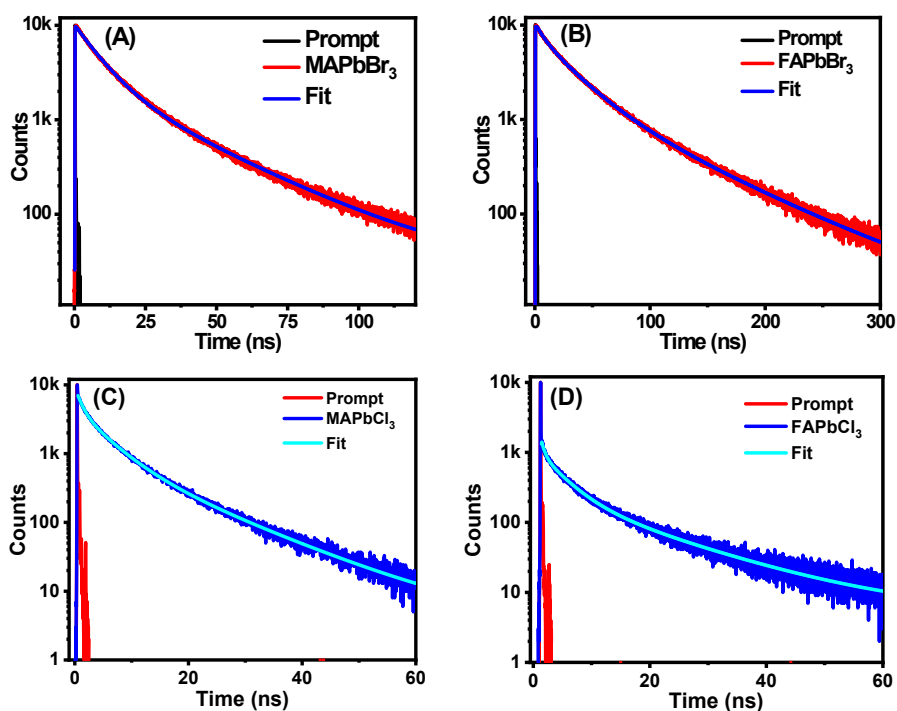


Fig. S13 PL decay characteristics of the (A) MAPbBr₃, (B) FAPbBr₃, (C) MAPbCl₃ and (D) FAPbCl₃ NCs. The excitation wavelengths are 405 and 376 nm for the bromide- and chloride-based NCs, respectively and the PL was monitored at their respective PL peak maxima. The early (short) component of the PL decay of FAPbCl₃ NCs could not be measured accurately as this component is shorter than the time-resolution of our TCSPC setup (~63 ps).

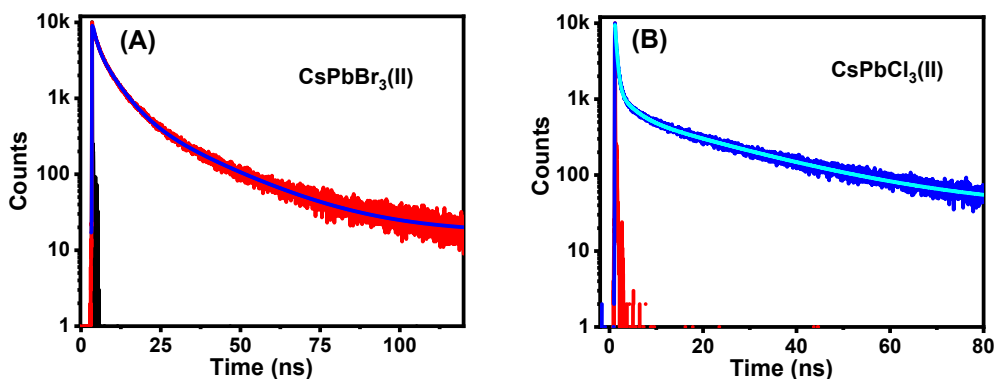


Fig. S14 PL decay of (A) CsPbBr₃(II) and (B) CsPbCl₃(II) NCs (prepared using Pb:X precursor molar ratio of 1:2). These samples were excited at 404 and 376 nm, respectively and the decay was monitored at the corresponding PL maxima.

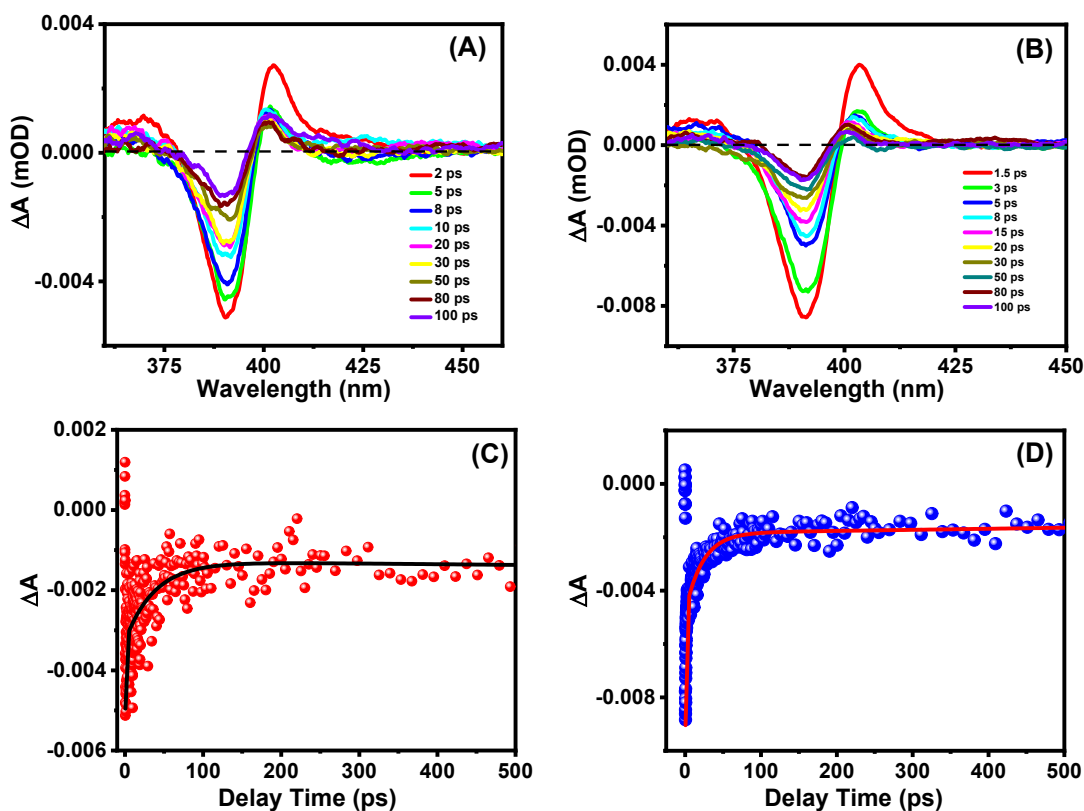


Fig. S15 TA spectra of (A) MAPbCl₃ and (B) FAPbCl₃ NCs obtained upon excitation at 350 nm by a fs-pulsed laser. Bleach recovery dynamics of (C) MAPbCl₃ and (D) FAPbCl₃ NCs monitored at their respective bleach maxima.

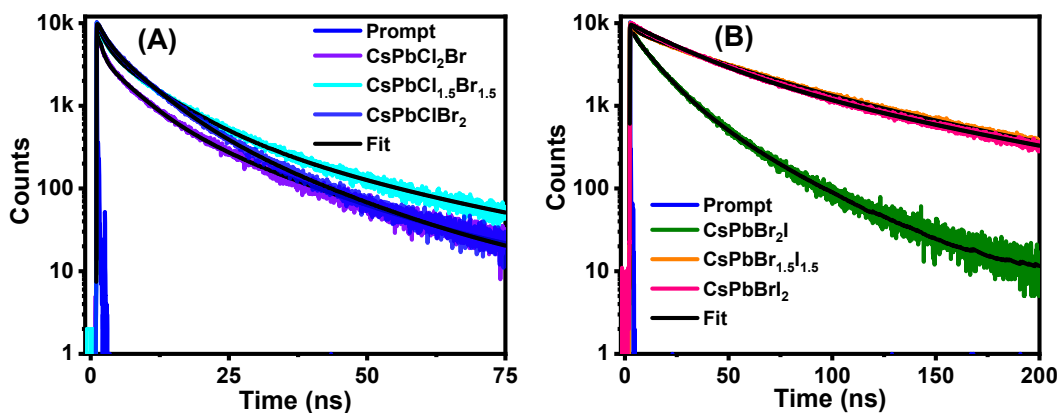


Fig. S16 PL decay behavior of the (A) blue-emitting CsPb(Cl/Br)₃ and (B) yellow-orange-emitting CsPb(Br/I)₃ NCs. The samples were excited at 375 and 405 nm, respectively and the decay curves were monitored at their respective peak maxima.

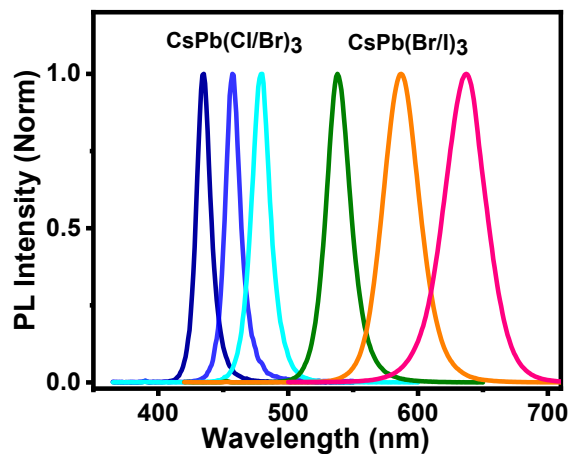


Fig. S17 (A) PL spectra (normalized) of our samples of mixed-halide NCs covering a wide (431 to 635 nm) range of the visible region.

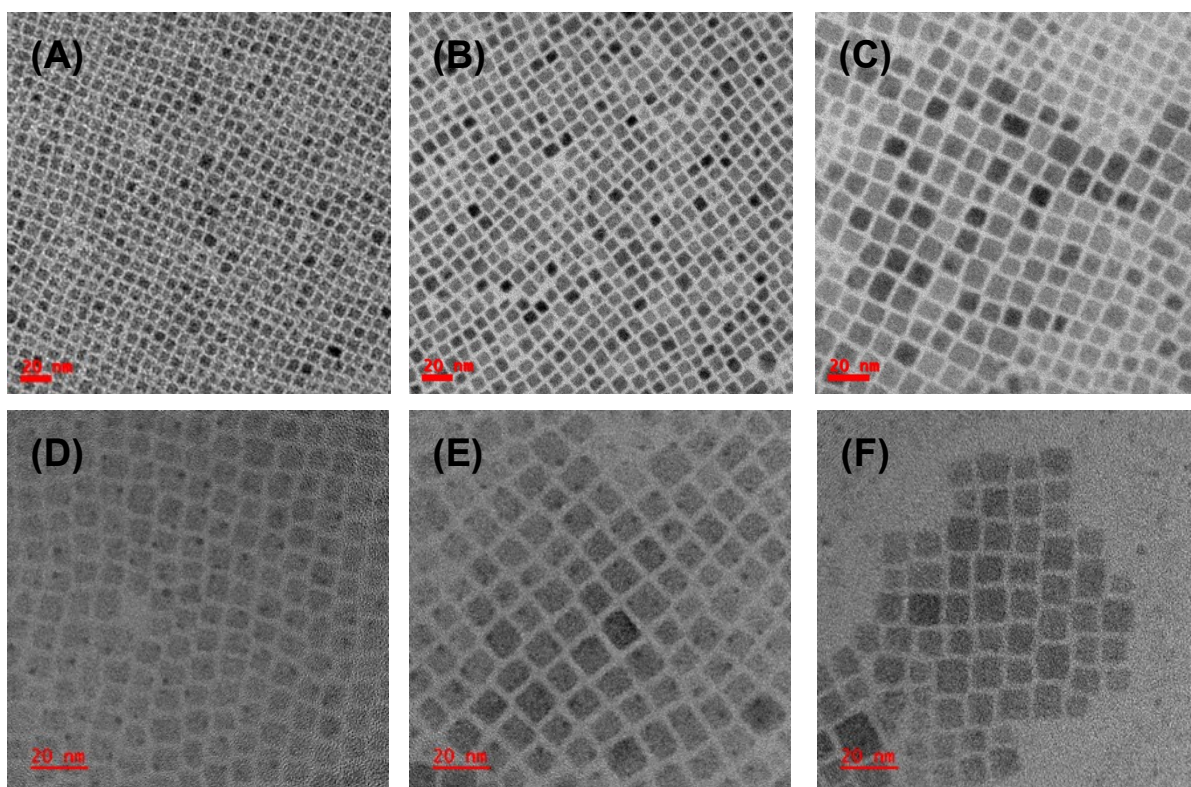


Fig. S18 Bright field TEM images (A) CsPbCl₂Br, (B) CsPbCl_{1.5}Br_{1.5}, (C) CsPbClBr₂, (D) CsPbBr₂I, (E) CsPbBr_{1.5}I_{1.5} and (F) CsPbBrI₂ NCs. The average edge lengths of the NCs are 6.9±1.4, 7.8±1.2, 9.3±2.2, 8.5±1.7, 9.4±2.5 and 10±2 nm, respectively.

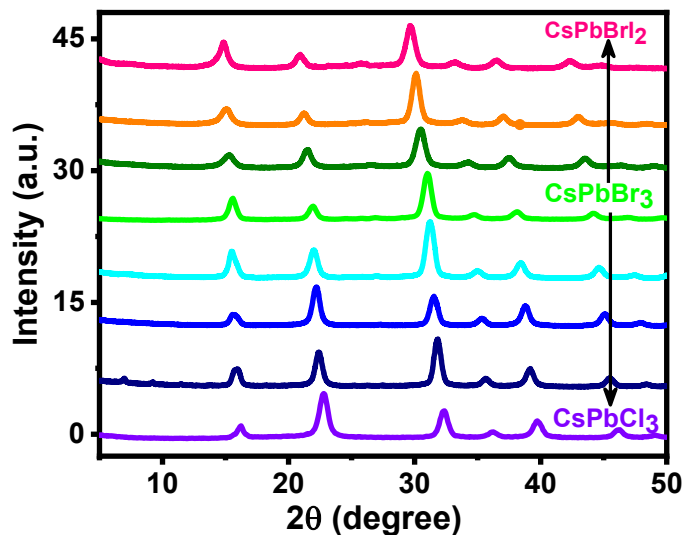


Fig. S19 XRD patterns of pristine CsPbCl₃, CsPbBr₃ and the mixed-halide CsPb(Cl/Br)₃ and CsPb(Br/I)₃ NCs.

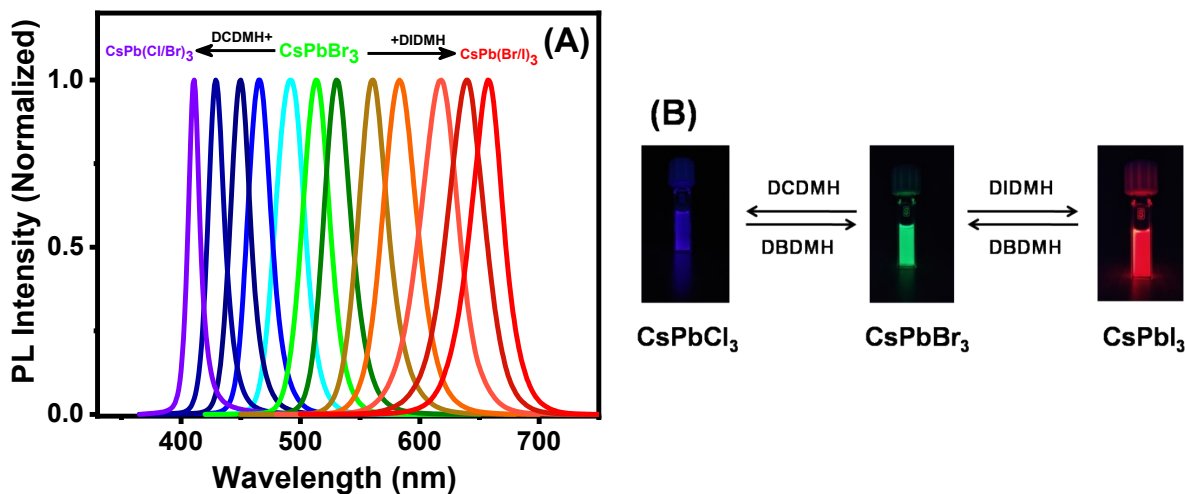


Fig. S20 (A) Addition of a small quantity of DCDMH/DIDMH solution (in OAm and OA) to a colloidal dispersion of CsPbBr₃ NCs results in an instantaneous blue/red shift of the PL maximum in the range of ~410 to 660 nm due to room-temperature post-synthetic reversible halide exchange on the NCs. (B) Digital images of the CsPbBr₃ NCs before and after halide exchange reactions.

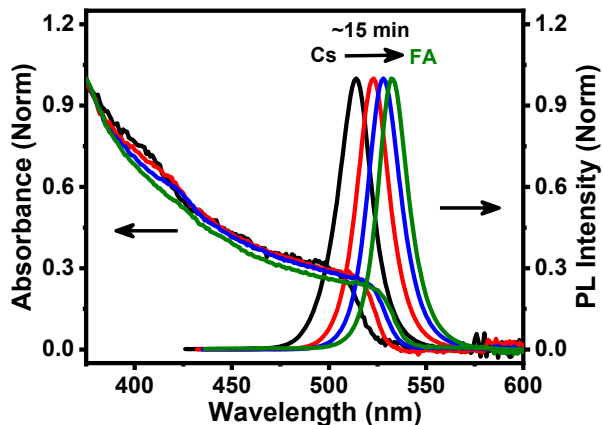


Fig. S21 Post-synthetic cation exchange (A-site) on CsPbBr₃ NCs using FA-oleate solution at RT.

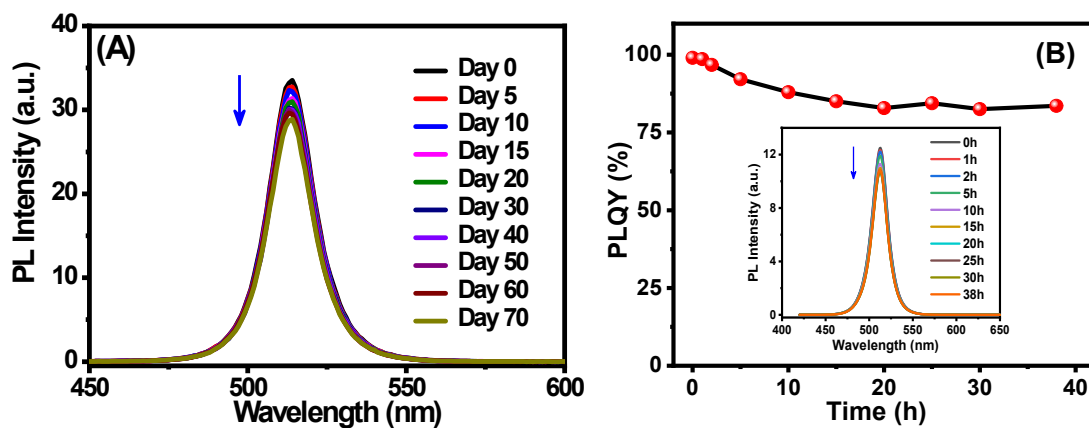


Fig. S22 (A) Change in PL spectrum of the CsPbBr₃ NCs with time (stored under ambient conditions). (B) Photoinduced change in the PLQY of the CsPbBr₃ NCs under continuous illumination of 365 nm UV light (8W). Inset shows the PL spectra of the sample during the testing period.

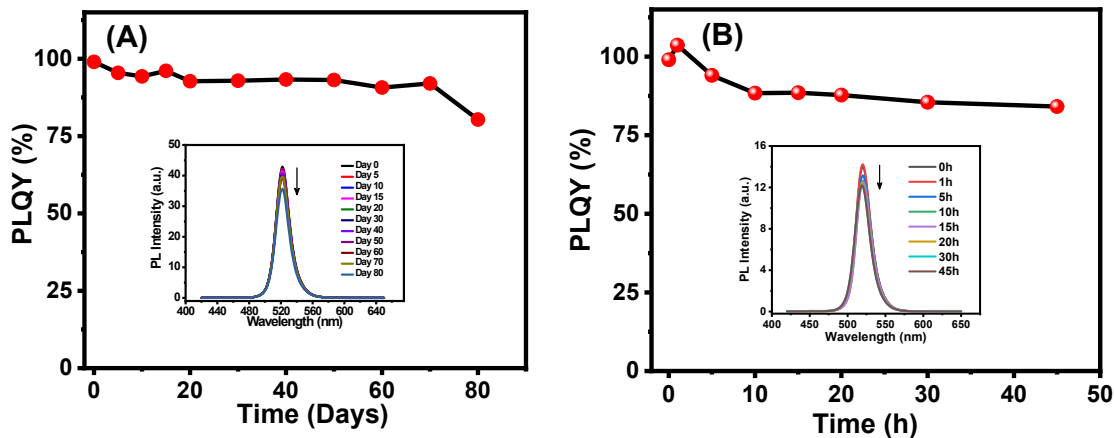


Fig. S23 Change in PL spectrum of the MAPbBr₃ NCs with time (stored under ambient conditions). (B) Photoinduced change in the PLQY of the MAPbBr₃ NCs under continuous illumination of 365 nm UV light (8W). Inset shows the PL spectra of the sample during the testing period.

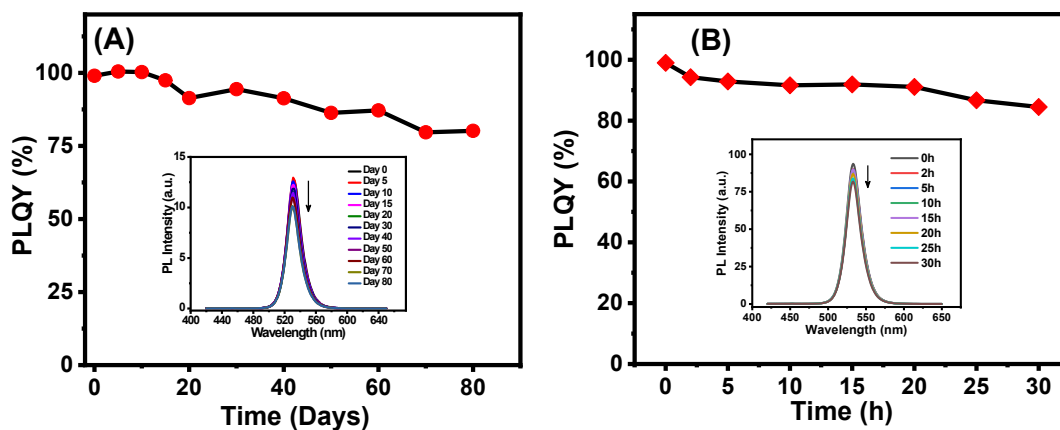


Fig. S24 Change in PL spectrum of the FAPbBr₃ NCs with time (stored under ambient conditions). (B) Photoinduced change in the PLQY of the FAPbBr₃ NCs under continuous illumination of 365 nm UV light (8W). Inset shows the PL spectra of the sample during the testing period.

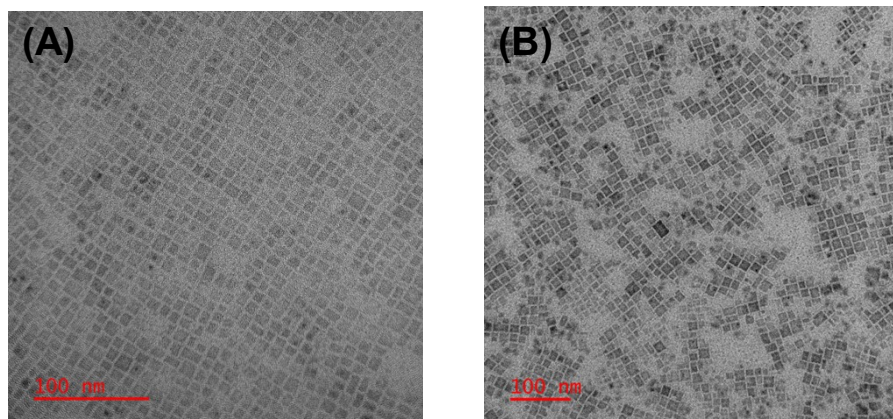


Fig. S25 Bright-field TEM images of the (A) MAPbBr₃, (B) FAPbBr₃ NCs taken after 80 days of storage under ambient condition. The scale bar is 100 nm in each image.

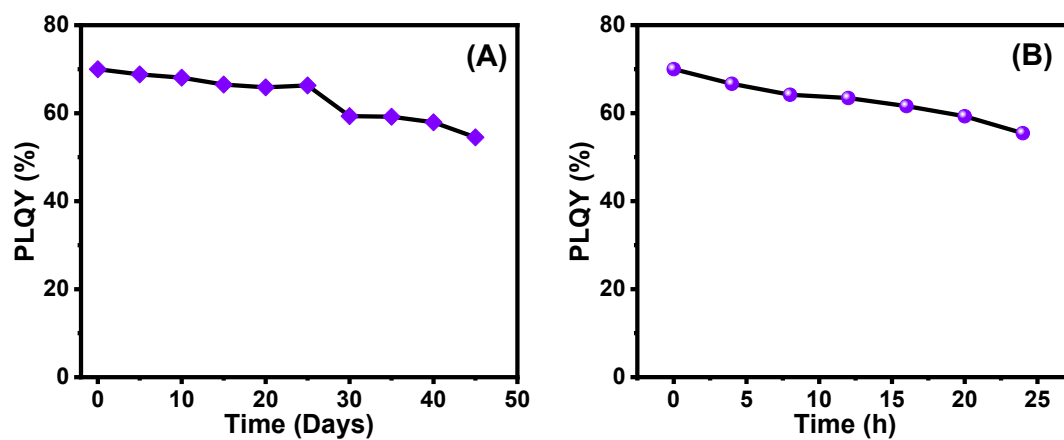


Fig. S26 Time-dependent change in PLQY of the CsPbCl₃ NCs under (A) ambient condition and (B) UV light (365 nm, 8W) illumination highlighting the air-stability and photo-stability of the samples.

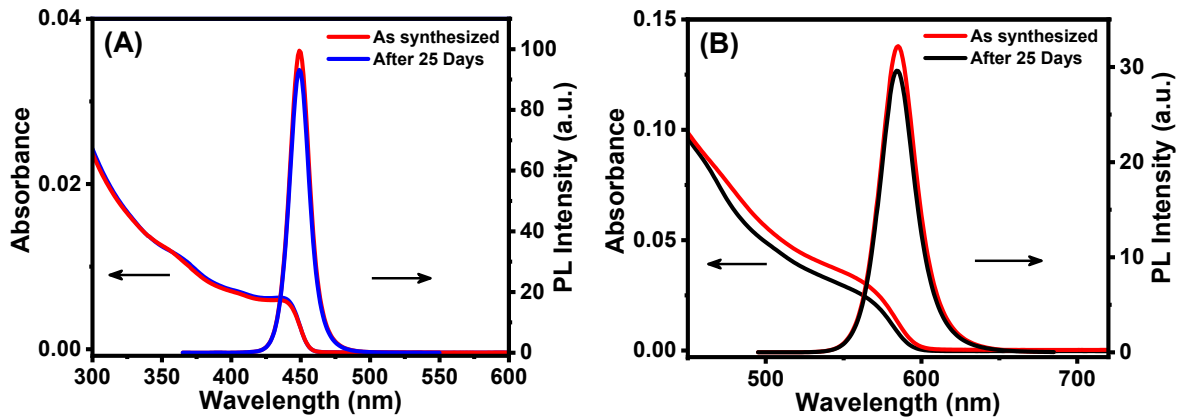


Fig. S27 Absorption and PL spectra of (A) CsPbCl_{1.5}Br_{1.5} and (B) CsPbBr_{1.5}I_{1.5} NCs recorded after storing under ambient conditions for 25 days.

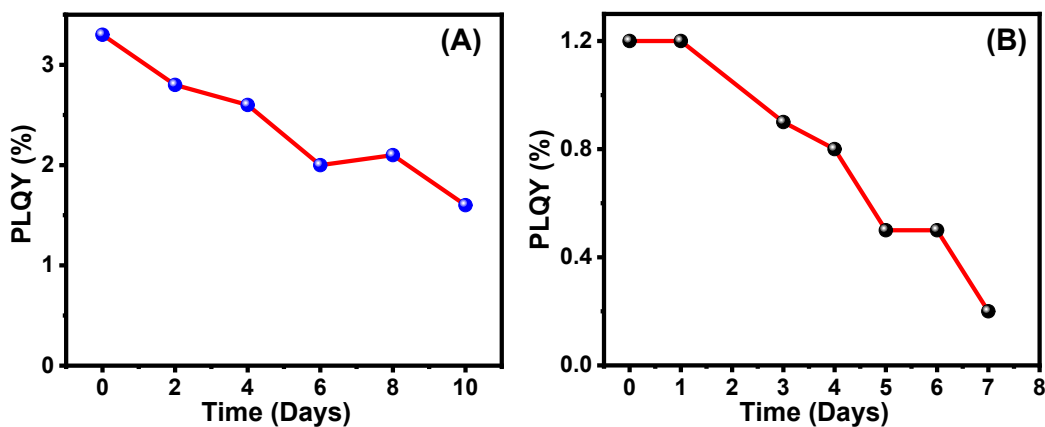


Fig. S28 Time dependent evolution of PLQY of (A) MAPbCl₃ and (B) FAPbCl₃ NCs under ambient condition.

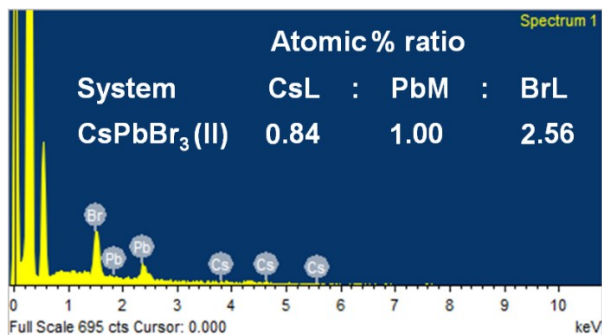


Fig. S29 EDX spectrum of the CsPbBr₃(II) NCs. The atomic % ratio of the constituting elements is indicated in the panel.

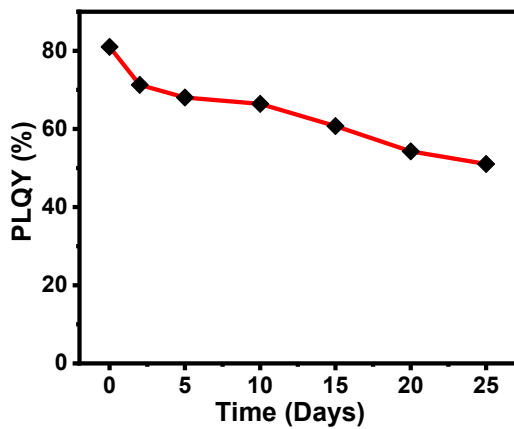


Fig. S30 Time-dependent change in PLQY of the CsPbBr₃(II) NCs stored under ambient condition.

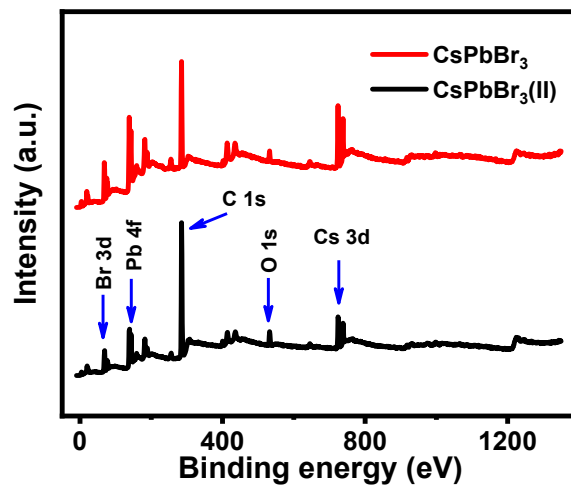


Fig. S31 XPS general survey scans of the CsPbBr_3 and $\text{CsPbBr}_3(\text{II})$ NCs indicating the presence of all constituent elements in both samples. Both spectra were corrected with respect to C 1s peak at 285.0 eV.

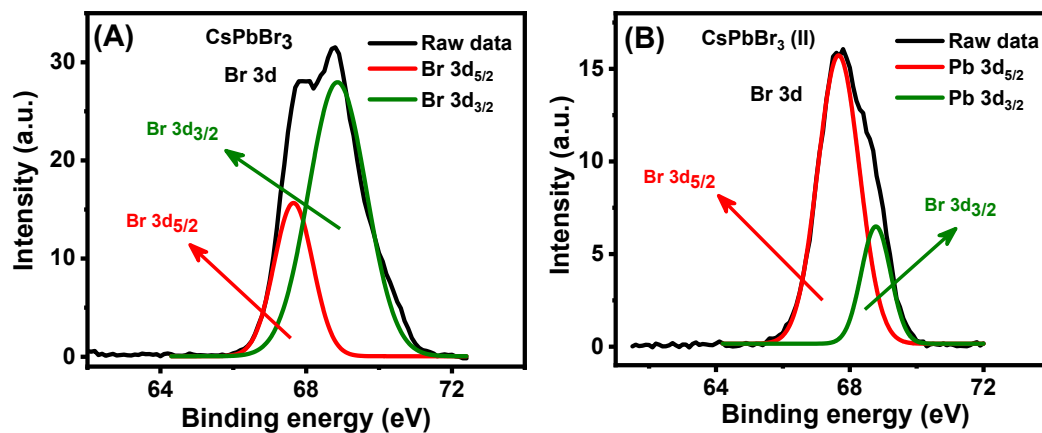


Fig. S32 Core-level XPS spectra of Br 3d of (A) CsPbBr_3 and (B) $\text{CsPbBr}_3(\text{II})$ NCs.

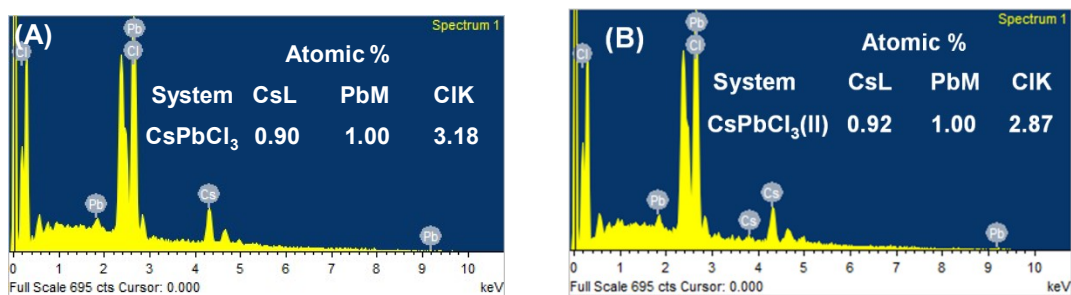


Fig. S33 EDX spectra of (A) CsPbCl₃ and (B) CsPbCl₃(II) NCs. Atomic % ratios of the NCs are shown in the panels.

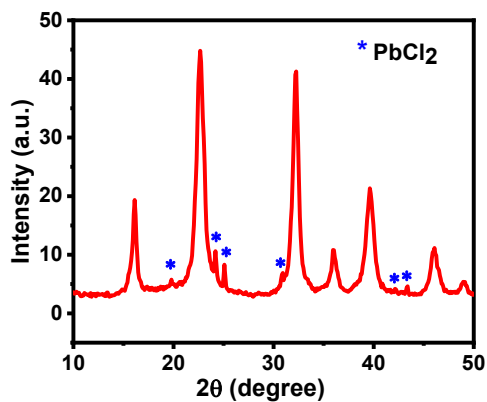


Fig. S34 PXRD spectra of CsPbCl₃ NCs prepared with Pb:Cl molar ratio of 1:9. (*) represent PbCl₂ diffraction peaks.

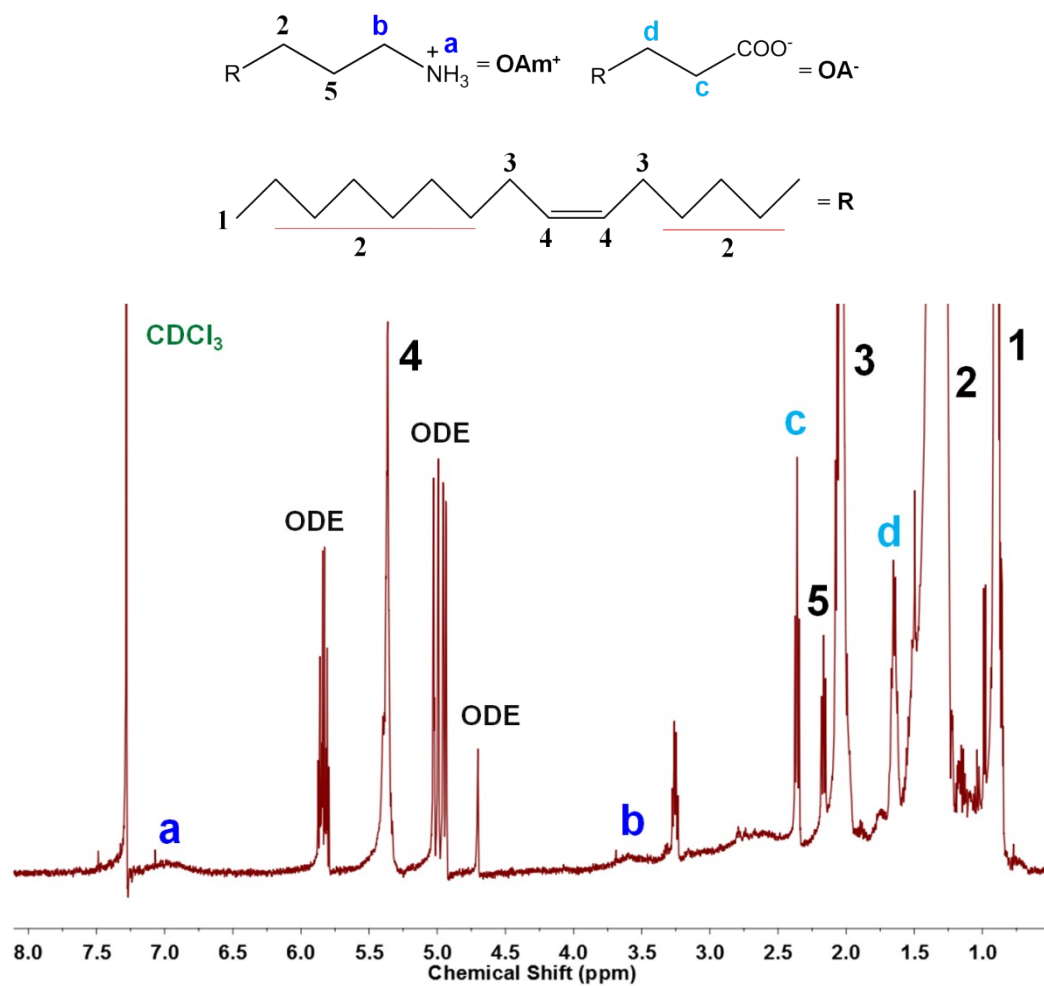


Fig. S35 ^1H NMR spectrum of purified CsPbBr_3 NCs in CDCl_3 .

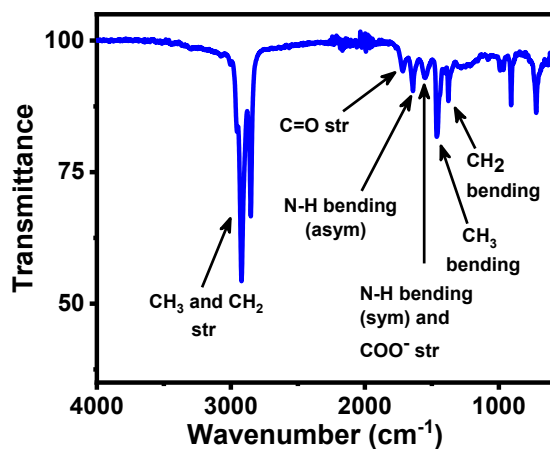


Fig. S36 FTIR spectrum of purified CsPbBr₃ NCs in hexane.

Table S1: Dependence of the optical properties of the APbX₃ NCs on reaction temperature and Pb:X precursor molar ratio.

Systems	Pb:X	Temperature (°C)	PLQY (±2 %)	FWHM (nm)
CsPbBr ₃	1:3	165, 180, 200 and 210	66, 80, 91 and 99	26, 23, 20 and 19
MAPbBr ₃	1:3	130, 150 and 165	52, 79 and 99	55, 26 and 21
FAPbBr ₃	1:3	130, 150 and 165	68, 86, 99	29, 24 and 19
CsPbCl ₃	1:3	165, 180, 200 and 210	39, 56, 64 and 70	14-10
CsPbBr ₃ (II)	1:2	210	81	20
CsPbCl ₃ (II)	1:2	210	36	11

Table S2: Comparison of the PLQY of violet-emitting CsPbCl₃ NCs obtained by different methods of direct synthesis.

System	Pb:Cl ratio	PLQY (%)	λ_{em} (nm)	References
CsPbCl ₃	1:(5.5-6.6)	97	411	8
	1:9	65	408	9
	1:4.5	71	404	10
	1:9	80	404	11
	1.3	70±2	406	This work

Table S3: PL decay parameters, radiative (k_r) and non-radiative (k_{nr}) rate constants of the APbX₃ NCs. The decay was monitored at the respective PL maximum after excitation at 375 nm (for violet-blue-emitting), 404 nm (for green-emitting) and 485 nm (for yellow-orange-emitting) samples. The k_r and k_{nr} values were calculated using $k_r = \text{PLQY}/\langle\tau_{amp}\rangle$ and $k_{nr} = (1 - \text{PLQY})/\langle\tau_{amp}\rangle$.

Systems	Pb:X ratio	$\tau_1(a_1)$ [ns]	$\tau_2(a_2)$ [ns]	$\tau_2(a_2)$ [ns]	$\langle\tau_{amp}\rangle$ [ns]	k_r [ns ⁻¹]	k_{nr} [ns ⁻¹]
CsPbBr ₃	1:3	4.97 (0.73)	12.50 (0.27)	---	7.0	0.14	0.001
CsPbBr ₃ (II)	1:2	5.31 (0.42)	20.65 (0.08)	0.61 (0.50)	4.18	0.18	0.057
MAPbBr ₃	1:3	8.50 (0.74)	29.20 (0.26)	---	13.88	0.07	0.0007
FAPbBr ₃	1:3	21.02 (0.68)	65.80 (0.32)	---	35.35	0.03	0.0003
CsPbCl ₃	1:3	4.63 (0.19)	20.72 (0.05)	0.47 (0.76)	2.48	0.28	0.120
CsPbCl ₃ (II)	1:2	3.67 (0.07)	18.05 (0.07)	0.40 (0.86)	1.86	0.19	0.344
MAPbCl ₃	1:1.5	4.52 (0.43)	12.79 (0.13)	1.05 (0.44)	4.10	0.008	0.240
FAPbCl ₃	1:3	3.90 (0.45)	15.39 (0.15)	0.59 (0.40)	4.30	0.003	0.229

Table S4: Kinetic parameters of the bleach recovery dynamics of different samples of CsPbBr₃ and CsPbCl₃ NCs.

Samples	Pb:X	τ_1 (a₁)/ps	τ_2 (a₂)/ps	τ_3 (a₃)/ps
CsPbBr ₃	1:3		>1000	
CsPbBr ₃ (II)	1:2	53.2 (0.43)	>1000 (0.57)	
CsPbCl ₃	1:3	5.9±1.6 (0.31)		>1000 (0.69)
CsPbCl ₃ (II)	1:2	5.8±0.3 (0.29)	74.8±5 (0.56)	>1000 (0.15)
MAPbCl ₃	1:1.5	2.9±1.0 (0.60)	36.3±3.5 (0.26)	>1000 (0.14)
FAPbCl ₃	1:3	2.1±0.4 (0.56)	20±2.2 (0.33)	>1000 (0.11)

Table S5: Amount of DCDMH, DBDMH or DIDMH taken for the synthesis of mixed-halide NCs at 210°C.

Systems	Pb:X ratio	X:X' ratio	DCDMH/mg	DBDMH/mg	DIDMH/mg
CsPbCl ₂ Br	1:3	2:1	74.08	53.75	---
CsPbCl _{1.5} Br _{1.5}	1:3	1.5:1.5	55.56	80.63	---
CsPbClBr ₂	1:3	1:2	37.04	107.51	---
CsPbBr ₂ I	1:3	2:1	---	107.51	71.42
CsPbBr _{1.5} I _{1.5}	1:3	1.5:1.5	---	80.63	107.14
CsPbBrI ₂	1:3	2:1	---	53.75	142.85

Table S6: Optical properties of various mixed-halide CsPb(Cl/Br)₃ and CsPb(Br/I)₃ NCs.

Systems	λ_{em} (nm)	PLQY (%)	FWHM (nm)
CsPbCl ₂ Br	431±2	87±1	12
CsPbCl _{1.5} Br _{1.5}	458±2	95±1	13
CsPbClBr ₂	478±2	96±1	15
CsPbBr ₂ I	531±2	68±2	21
CsPbBr _{1.5} I _{1.5}	584±2	86±2	32
CsPbBrI ₂	635±2	98±1	37

Table S7: Comparison of the optical properties of different mixed-halide systems obtained directly by different methods.

Systems	Synthetic strategy	Method	PLQY (%)	PL peak / FWHM (nm)	Ref.
CsPbCl ₃ CsPbCl _{1.5} Br _{1.5} CsPbClBr ₂	PbX ₂ as lead and halide source	LARP	10	10/12	12
			37	455/16	
			70	478/18	
CsPbBr ₂ I CsPbBr _{1.5} I _{1.5} CsPbBr _{1.2} I _{1.8} CsPbBrI ₂			78	548/26	
			72	600/38	
			80	628/35	
			70	640/35	
CsPb(Br _{1-x} Cl _x) ₃ Where x= 0-0.39	Quaternary alkyl ammonium halides as additional halide source with PbX ₂	HI	25 (x = 0.39) 32 (x = 0.24) 48 (x = 0.19) 62 (x = 0.11) 80 (x = 0)	462 476 487 499 510 FWHM= 18-20	13
CsPbCl ₃ CsPbCl ₂ Br CsPbCl _{1.5} Br _{1.5} CsPbClBr ₂ CsPbBr ₃	N-chloro- and N-bromophthalimides as halide precursors	HI	80 85 92 97 99	404/9 428/14 447/15 475/17 510/20	11
CsPbCl ₂ Br CsPbCl _{1.5} Br _{1.5} CsPbClBr ₂ CsPbBr ₂ I CsPbBr _{1.5} I _{1.5} CsPbBrI ₂	DHDMH as halide precursor	HI	87±1 95±1 96±1 68±2 86±2 98±1	431±2/12 458±2/13 478±2/15 531±2/21 584±2/32 635±2/37	This work

Table S8: PL decay components of different mixed-halide samples of CsPb(Cl/Br)₃ and CsPb(Br/I)₃ NCs.

Systems	$\tau_1(a_1)/\text{ns}$	$\tau_2(a_2)/\text{ns}$	$\tau_3(a_3)/\text{ns}$	$\langle\tau_{\text{amp}}\rangle/\text{ns}$	k_r/ns^{-1}	$k_{\text{nr}}/\text{ns}^{-1}$
CsPbCl ₂ Br	5.37(0.34)	17.32(0.09)	0.71(0.57)	3.79	0.23	0.03
CsPbCl _{1.5} Br _{1.5}	7.78(0.43)	24.20(0.08)	1.53(0.49)	6.03	0.16	0.008
CsPbClBr ₂	6.14(0.54)	16.60(0.10)	1.5(0.36)	5.52	0.17	0.007
CsPbBr ₂ I	11.30(0.53)	30.90(0.17)	0.94(0.30)	11.52	0.06	0.03
CsPbBr _{1.5} I _{1.5}	34.20(0.50)	88.60(0.30)	2.44(0.20)	44.17	0.02	0.003
CsPbBrI ₂	27.30(0.69)	84.60(0.31)	---	45.06	0.02	0.0004

Table S9: Comparison of the optical properties and stability of the green- and violet-emitting perovskite NCs obtained by different three-precursor method of synthesis.

Systems	Halide precursor	PLQY (%)/ FWHM (nm)	Stability parameters	References
FAPbBr ₃	Oleylammonium bromide	85/22	Stable up to 2-3 round of purification with ACN	2
CsPbBr ₃	Tetraoctyl ammonium bromide	78	~20 % PLQY retained after 35 days in air and ~24% PLQY reduced after 3 heating-cooling circle at 100°C	14
CsPbBr ₃	Tetraoctyl ammonium bromide	70	Stable towards purification with polar solvents up to 2 times	15

CsPbBr ₃	NH ₄ Br	75/19	Stable towards purification	16
FAPbBr ₃	Octadecylamine bromide	88/21	~75% retention of PLQY after 50 days of storage in air	17
CsPbBr ₃ MAPbBr ₃ FAPbBr ₃ CsPbCl ₃	Benzoyl halide	92/18 92/19 92/20	NA	9
CsPbBr ₃	Trioctylphosphene-Br ₂ adduct	90/17	PLQY retained in the range of 70-90% for 28-50 days	18
CsPbBr ₃	Benzoyl halide	48-80/16-17	NA	19
CsPbCl ₃	Oleylammonium halide	97	80% PLQY retained after 7 days	8
CsPbBr ₃		97	NA	
CsPbBr ₃ MAPbBr ₃ FAPbBr ₃	N-bromosuccinamide	99/18 98/21 95/20	<p><i>Air-stability:</i> CsPbBr₃ retains 90% while MAPbBr₃ and FAPbBr₃ retains 85% of initial PLQY after 3 and 2 months in air, respectively</p> <p><i>Photo-stability:</i> CsPbBr₃, MAPbBr₃ and FAPbBr₃ retains 81, 75 and 80% of their initial PL intensity after 24h of UV illumination</p> <p><i>Polar solvent stability:</i> CsPbBr₃ NCs retains 70% of its initial PL intensity after 24h in presence of water</p>	20
CsPbBr ₃	Bromopropane	78.5/18.2	Initial PLQY reduced by 17% in air after 120 days and retained 67.85% under UV light for 96 h	21
CsPbCl ₃	Phenylphosphonic	71/12	80% and 50% of initial PLQY retained after 5h under UV light and	10

	dichloride		10 rounds of purification	
CsPbCl ₃	N-halophthalimide as halide source	80/9	<i>Air-stability</i> : Retention of 85% PLQY after 2 weeks in ambient condition	11
CsPbBr ₃		99/20	NA	
CsPbBr ₃ MAPbBr ₃ FAPbBr ₃	1,3-dihalo-5,5-dimethylhydantoin	99/19 99/21 99/20	<i>Air-stability</i> : ~80-85% of initial PL intensity retained after 70-80 days of storage under ambient condition <i>Photo-stability</i> : ~85% of initial PLQY restored after >30h of continuous UV irradiation <i>Polar solvent stability</i> : ~80% of initial PL intensity retained even after 24h in presence of water	This work
CsPbCl ₃		70/10	<i>Air/Photo-stability</i> : ~80% of initial PLQY retained after 45 days in ambient condition and under 24h UV irradiation, respectively.	

Table S10: Advantages and disadvantages of different halide precursor used in hot-injection method of synthesis.

Halide Precursor	Advantage	Disadvantage/s	Ref.
PbX_2 (X= Cl, Br and I)	Most frequently used halide and lead precursor	Difficult to control composition of the final NCs due to sub-stoichiometric amount of halogen and the formed halide-deficient NCs show poor stability and optical properties.	1, 2, 22
OAm^+X^- (X= Cl, Br and I)	All three all-inorganic $CsPbX_3$ NCs with near-unity PLQY can be prepared. Produces good quality $FAPbX_3$ (X= Br and I) NCs with high stability.	Highly hygroscopic and hence, special protection is needed for storing the samples. Systems like $MAPbX_3$ and $FAPbCl_3$ NCs are not reported yet. In some cases, the NCs are moderately stable under ambient condition (1-2 weeks).	2, 8, 23, 24
Benzoyl halides	All $APbX_3$ NCs can be obtained. The green-emitting $APbBr_3$ shows PLQY of ~92% and the violet/red-emitting $CsPbCl_3$ and $CsPbI_3$ NCs show PLQY of ~65 and 58%, respectively. The $CsPbI_3$ NCs are stable for over 20 days under ambient condition.	The iodide-based NCs are moderately luminescent (PLQY between 45-58%). Except $CsPbI_3$ NCs, stability of the other systems are not examined. Optical properties and stability of the mixed-halide NCs are not explored. Benzoyl halides are highly toxic.	9
NXI_m (X= Cl, Br)	High quality $APbBr_3$ NCs with near-unity PLQY can be prepared with exceptional stability under ambient condition. Blue-emitting NCs with PLQY of 85-97% and violet-emitting $CsPbCl_3$ NCs with second highest value of PLQY of 80% can be prepared.	Many systems like chloride and iodide-based hybrid NCs and yellow/orange-emitting mixed-halide NCs could not be obtained. The $CsPbI_3$ NCs are weakly luminescent (PLQY ~27%) and stable only for a few days.	11, 20

DBDMH	PLQY of the APBr ₃ NCs between ~91-95% can be prepared.	Only the green-emitting NCs are formed. Stability of the NCs is moderate.	25
DXDMH (X= Cl, Br and I)	APbBr ₃ NCs exhibit near-unity PLQY with excellent stability. Red/NIR-emitting APbI ₃ NCs exhibit high phase stability for several months and possess PLQY in the range of 67-96%, highest by any common method till date. PLQYs of the mixed-halide NCs are comparable or better than any previous method. Provides a common method of achieving high quality all APbX ₃ NCs emitting across the visible (extendable to NIR) region.	Violet-emitting MAPbCl ₃ and FAPbCl ₃ NCs exhibit poor optical properties and stability. PLQY of CsPbCl ₃ , MAPbI ₃ and FAPbI ₃ NCs are less than unity. Size control of the NCs was unsuccessful.	This work

Table S11: Atomic % ratio of the constituting elements (Cs, Pb and Br) and nitrogen (N) in CsPbBr₃ NCs obtained from XPS measurement.

Samples	Area under the curve/ASF				Atomic % ratio (with respect to Pb)			
	Cs	Pb	Br	N	Cs	Pb	Br	N
CsPbBr ₃	24948.45	29153.57	91152.43	53351.03	0.85	1.00	3.13	1.83
CsPbBr ₃ (II)	18149.36	19481.49	52471.89	28248.16	0.93	1.00	2.69	1.45

Table S12: Atomic % ratio of Cs, Pb and Cl in CsPbCl₃ NCs obtained with different Pb:Cl precursor molar ratio.

Pb:Cl molar ratio	Atomic % ratio		
	CsL	PbM	ClK
1:3	0.90	1.00	3.18
1:5	0.88	1.00	3.19
1:7	0.91	1.00	3.16
1:9	0.95	1.00	3.05

References:

1. L. Protesescu, S. Yakunin, M. I. Bodnarchuk, F. Krieg, R. Caputo, C. H. Hendon, R. X. Yang, A. Walsh and M. V. Kovalenko, *Nano Lett.*, 2015, **15**, 3692–3696.
2. L. Protesescu, S. Yakunin, M. I. Bodnarchuk, F. Bertolotti, N. Masciocchi, A. Guagliardi and M. V. Kovalenko, *J. Am. Chem. Soc.*, 2016, **138**, 14202–14205.
3. A. De, S. Das and A. Samanta, *ACS Energy Lett.*, 2020, **5**, 2246–2252.
4. N. Mondal and A. Samanta, *Nanoscale*, 2017, **9**, 1878-1885.
5. A. Maciejewski and R. P. Steer, *Journal of Photochemistry*, 1986, **35**, 59-69.
6. K. Rurack and M. Spieles, *Anal. Chem.*, 2011, **83**, 1232–1242.
7. R.F.Kubin and A.N.Fletcher, *J. Lumin.*, 1982, **27**, 455-462.
8. A. Dutta, R. K. Behera, P. Pal, P. D. S. Baitalik and D. N. Pradhan, *Angew. Chem. Int. Ed.*, 2019, **58**, 5552 –5556.
9. M. Imran, V. Caligiuri, M. Wang, L. Goldoni, M. Prato, R. Krahne, L. D. Trizio and L. Manna, *J. Am. Chem. Soc.*, 2018, **140**, 2656–2664.
10. C. Zhang, Q. Wan, L. K. Ono, Y. Liu, W. Zheng, Q. Zhang, M. Liu, L. Kong, L. Li and Y. Qi, *ACS Energy Lett.*, 2021, **6**, 3545–3554.
11. S. Paul, T. Ahmed, S. Das and A. Samanta, *J. Phys. Chem. C*, 2021, **125**, 23539–23547.
12. X. Li, Y. Wu, S. Zhang, B. Cai, Y. Gu, J. Song and H. Zeng, *Adv. Funct. Mater.*, 2016, **26**, 2435–2445.
13. Y. Shynkarenko, M. I. Bodnarchuk, C. Bernasconi, Y. Berezovska, V. Verteletskyi, S. T. Ochsenbein and M. V. Kovalenko, *ACS Energy Lett.*, 2019, **4**, 2703–2711.
14. S. Wei, Y. Yang, X. Kang, L. Wang, L. Huang and D. Pan, *Chem. Commun.*, 2016, **52**, 7265-7268.
15. E. Yassitepe, Z. Yang, O. Voznyy, Y. Kim, G. Walters, J. A. Castañeda, P. Kanjanaboos, M. Yuan, X. Gong, F. Fan, J. Pan, S. Hoogland, R. Comin, O. M. Bakr, L. A. Padilha, F. Nogueira and E. H. Sargent, *Adv. Funct. Mater.*, 2016, **26**, 8757–8763.

16. P. Liu, W. Chen, W. Wang, B. Xu, D. Wu, J. Hao, W. Cao, F. Fang, Y. Li, Y. Zeng, R. Pan, S. Chen, W. Cao, X. W. Sun and K. Wang, *Chem. Mater.*, 2017, **29**, 5168–5173.
17. Q. Li, H. Li, H. Shen, F. Wang, F. Zhao, F. Li, X. Zhang, D. Li, X. Jin and W. Sun, *ACS Photonics*, 2018, **4**, 2504–2512.
18. F. Krieg, S. T. Ochsenein, S. Yakunin, S. t. Brinck, P. Aellen, A. Süess, B. Clerc, D. Guggisberg, O. Nazarenko, Y. Shynkarenko, S. Kumar, C.-J. Shih, I. Infante and M. V. Kovalenko, *ACS Energy Lett.*, 2018, **3**, 641–646.
19. M. Imran, P. Ijaz, D. Baranov, L. Goldoni, U. Petralanda, Q. Akkerman, A. L. Abdelhady, M. Prato, P. Bianchini, I. Infante and L. Manna, *Nano Lett.*, 2018, **18**, 7822–7831.
20. S. Paul and A. Samanta, *ACS Energy Lett.*, 2020, **5**, 64–69.
21. S. Akhil, V. G. V. Dutt and N. Mishra, *Nanoscale*, 2021, **13**, 13142–13151.
22. O. Vybornyi, S. Yakunin and M. V. Kovalenko, *Nanoscale*, 2016, **8**, 6278–6283.
23. Q. A. Akkerman, L. Martínez-Sarti, L. Goldoni, M. Imran, D. Baranov, H. J. Bolink, F. Palazon and L. Manna, *Chem. Mater.*, 2018, **30**, 6915–6921.
24. L. Protesescu, S. Yakunin, S. Kumar, J. Bär, F. Bertolotti, N. Masciocchi, A. Guagliardi, M. Grotevent, I. Shorubalko, M. I. Bodnarchuk, C.-J. Shih and M. V. Kovalenko, *ACS Nano*, 2017, **11**, 3119–3134.
25. S. K. Mahankudo, A. Das, K. Mishra, M. Barai, P. Mal and S. Ghosh, *ACS Appl. Nano Mater.*, 2022, **5**, 4360–4366.